M. Belan
*Plasma-Gas Flow Interaction of a Discharge Normal to a Bluff Body Wake*
IEEE Transactions on Plasma Science, Vol. 42, N. 9, 2014, p. 2170-2178
doi:10.1109/TPS.2014.2342031

# Plasma–gas flow interaction of a discharge normal to a bluff body wake.

Marco Belan

***Abstract*—This work describes the interaction of a gas discharge with an air flow consisting of the wake of a flat plate normal to the airstream. The plate acts both as a bluff body and as a discharge electrode; the free discharge in the absence of the airstream and the free airstream without discharge are orthogonal to each other. The electric forces involved in the free discharge and the inertial forces involved in the free airstream are of the same order. The experiment has been carried out in a suitable duct, and the facilities include devices for discharge current measurements, a hot wire anemometer and a visualization system. The analysis of the time histories obtained from the hot wire signals and from the cathodic current signals reveals the existence of an airstream–discharge coupling phenomenon, appearing as synchronized oscillations of the flow and the discharge current.**

***Index Terms*—Fluid dynamics, plasma–gas flow interaction, streamer discharge**

## I. Introduction

GAS discharges can take many different forms under the large variety of possible conditions. The discharge corresponding to a non-thermal plasma stream in a ionized region of a gas, generically known as 'corona discharge', has been considered particularly important by engineers and physicists for many years [1]–[5]. The term 'corona' is generally used as a collective name for different discharge regimes always characterized by ions having temperatures typically close to the ambient value; particularly important are the glow (or proper corona) regime where the discharge fills a wide spatial region and the streamer (or filamentary) regime where the discharge consists of small pulsed channels of plasma. These regimes have been extensively studied, their volt-ampere characteristics are known for the most common electrodes geometries [5]–[7], as well as their transient processes and natural pulsation frequencies, that appear even if the discharge is DC-driven, for both polarities [8]–[12].

The corona discharge has several chemical, environmental and even bio-medical applications [13]; it can induce a gas flow known as electric wind, which gives rise to other important industrial applications. For example, the electric wind as it is can be used to design microblowers for the purpose of heat dissipation, but it is also capable of modifying an existing airflow, and in general a DC or AC discharge can be used for the sake of controlling a flow. Actually, a wide range of studies is devoted to flow and turbulence control through plasma-based devices, as outlined by Moreau [14].

M. Belan is with the Politecnico di Milano, Dipartimento di Scienze e Tecnologie Aerospaziali, via La Masa 34 - 20156 Milano, Italy; e-mail: marco.belan@polimi.it (see http://www.aero.polimi.it/belan).

Manuscript received .....

However, the study of the possible plasma–airflow interactions is a wider field of research, including the 'symmetric' problem of plasma control by means of an airflow, and the general problem of mutual interaction without control. The relevant literature includes many theoretical, experimental and numerical results, for AC as well as for DC discharges (for a small sample of interesting cases, see [15]–[21]). In general, the airstream–discharge interaction takes place on a volume where specific forces and energies can be easily identified; for instance, in flow control applications, even when a small energy can control a large flow, the energy density of the discharge is definitely higher than the airstream energy density in a small but important region of interaction. As the energies of the airflow and the discharge change, the relevant physics can exhibit very different properties; in particular, the appearance of an unsteady behaviour in the discharge may lead to complicated interactions with the airflow, which is in general characterized by different scales for its unsteady phenomena.

Within this range of possibilities, the experiment described in this work is an intermediate case, where the effects of the pure airstream and of the pure discharge are comparable. In particular, this experiment treats the interaction of the flow past a bluff body with a gas discharge. The body is a flat plate normal to the free stream, and it plays also the role of the discharge anode, whereas the cathode, positioned on a wall of the test section, is parallel to the free stream. The resulting configuration makes the main directions of airstream and discharge orthogonal each other. Furthermore, the discharge energy and the inertial energy of the airflow are kept to the same order of magnitude, as explained in §II. The setup is presented in §III, then the pure airflow and discharge are described in §IV. The resulting airflow–discharge interaction leads to the appearance of coupled oscillations in the wake and the discharge, described in detail in section §V and discussed in §VI.

## II. Physical background

The basic sketch of the plasma-flow interaction under study is shown in Fig. 1: the discharge is ignited between an anode (white plate) and a cathode (gray plate), over a volume schematically bounded by the dashed lines in figure, which is also in the field of motion of the airstream. The main directions of the electric field $\mathbf{E}$ and the air velocity $\mathbf{U}$, indicated in figure, are orthogonal each other. The span of the system is $L$, the size of the electrodes as well as their distance are in the order of $D$. On the 'effective' volume $D^2L$, the inertial force of the fluid having velocity $U$ and density $\rho$, has an order of

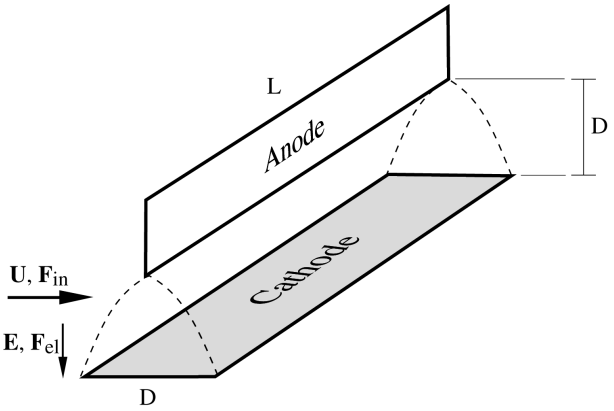


Fig. 1. Basic sketch of the interaction under study. The asymptotic velocity **U** is orthogonal to the central lines of the electric field **E**, the same holds for the relevant forces $\mathbf{F}_{el}$ and $\mathbf{F}_{in}$ considered in the dimensional analysis.

magnitude

$$F_{in} = \rho D L U^2 \tag{1}$$

and the electric force can be estimated as

$$F_{el} = qE\, n_i D^2 L = D\, i/\mu_i \tag{2}$$

where $q$ is the elementary charge, $n_i$ the number density of ions, $i$ the time-averaged discharge current and $\mu_i$ the ion mobility. Then, the ratio of discharge–induced body force to inertial force on a gas volume turns out to be

$$\frac{F_{el}}{F_{in}} = \frac{i}{\rho \mu_i\, U^2 L} = \frac{E_{hd}}{Re^2}, \tag{3}$$

where $E_{hd}$ is the *conductive electric Rayleigh number* or *EHD number* defined according to the international standards [4], [22],

$$E_{hd} = \frac{iD^2}{L\rho\mu_i\, \nu^2} = \frac{iD^3}{A\rho\mu_i\, \nu^2} \tag{4}$$

($A = LD$ is the area exposed to the discharge and $\nu$ the fluid viscosity) and the Reynolds number $Re$ is based on the scale $D$. The ratio (3) is also indicated as

$$N_{\mathrm{EHD}} = \frac{E_{hd}}{Re^2} \tag{5}$$

by some authors [14], [23], [24] and named *electrohydrodynamic number*, not to be confused with the EHD number defined above. The physical meaning of this quantity can be outlined observing that when $N_{\mathrm{EHD}} \ll 1$, the airflow is scarcely affected by the electric field, whereas $N_{\mathrm{EHD}} \gg 1$ indicates that the electric field dominates and may control the airflow, that is what happens in many plasma actuators. The products $F_{el}D$ and $F_{in}D$ may be used to estimate the energies involved in the same volume, so that the formula (3) can also be considered as an energy ratio. The present experiment is intentionally scaled in such a way as to keep $N_{\mathrm{EHD}}$ on an intermediate range; in particular, assuming ion mobilities in the order of $\mu_i \sim 2 \cdot 10^{-4}\mathrm{m}^2/(\mathrm{Vs})$, $N_{\mathrm{EHD}}$ lies typically in the range 0.01 to 0.75 and does not exceed 2.5 in any test. In this way, the discharge electric energy and the airflow kinetic energy are comparable, so that the physics is neither airflow-dominated nor discharge-dominated.

## III. Experimental Setup

In a realistic setup, the distance $D$ should be maintained in the cm range in order to avoid the use of enormous voltage values. However, the ignition voltage of a discharge remains in the kV range, and the current in a feasible experiment should be less than about 1 mA in order to limit the electric power and satisfy the similarity conditions exposed above. Assuming values of $\rho U^2$ well in the incompressible range, the last parameter to set in the definition of $N_{\mathrm{EHD}}$, after equations (3) and (5), is the length $L$. Keeping in mind that the electrical and inertial forces scale in different ways with the involved lengths, it turns out that the desired values of $N_{\mathrm{EHD}}$ can be achieved in a small size facility. The setup satisfying these requirements, modified from an earlier version by the same author [25], is shown in Fig. 2.

Here the airstream flows inside a duct with a test section of size $L \times H = 80 \times 50$ mm, hosting a metallic flat plate at $90°$ incidence. This plate spans the center of the section, parallel to the side of length $L$, it has a chord $c = 8$mm, a thickness of 0.5mm and is chamfered at both sides. The velocity during the present tests ranges from 3 to 6 m/s, so that the Reynolds number of the plate ranges approximately from 1500 to 3200 (this chord-based number is 0.4 times the Reynolds number defined in §II and based on gap $D$). The wake of the plate in the absence of the discharge is sketched in Fig. 2 by an averaged contour. At the regime under consideration, the wake is unsteady, with a moderate turbulence level, and its larger structures are vortices periodically shed from the plate sides, whose frequency is characterized in §IV-A below. Within this region the time-averaged values of the velocity are lower than the unperturbed value (velocity defect zone). At the duct walls, the velocity falls to zero within the thin boundary layer of the flow, having a size (displacement thickness) always less than 2.4mm.

The same plate is also connected to the positive pole of a DC high voltage generator through a ballast resistor, $R$ =2MΩ, and thanks to its sharp edges it can act as an anode of length $\sim L$, driven at voltages $V_0$ between 16 and 20kV. The maximum direct current available at the power supply is 0.5mA. The cathode consists of an array of plane electrodes, placed on a wall of the test section in order to give information about the spatial distribution of the discharge as a function of time. The contour of the discharge in the absence of the airstream is sketched in Fig. 2 as the zone including approximately 90% of the average total current; for the characterization of the pure discharge, see §IV-B. The extremities of the flat plate and of the cathodes along the $L$ direction, where the electric field becomes strongly nonuniform, are protected by suitable insulators. The cathodes are connected to ground through measuring devices having low impedances; depending on the particular test which is being performed, these devices can be low value resistors, current probes or transformers. The data presented in this work are acquired by reading the voltages across 10kΩ load resistors. The total capacitance of the electrodes, including the connection cables, is 320±10pF. The output signals are digitally acquired by devices sampling up to 100kHz.

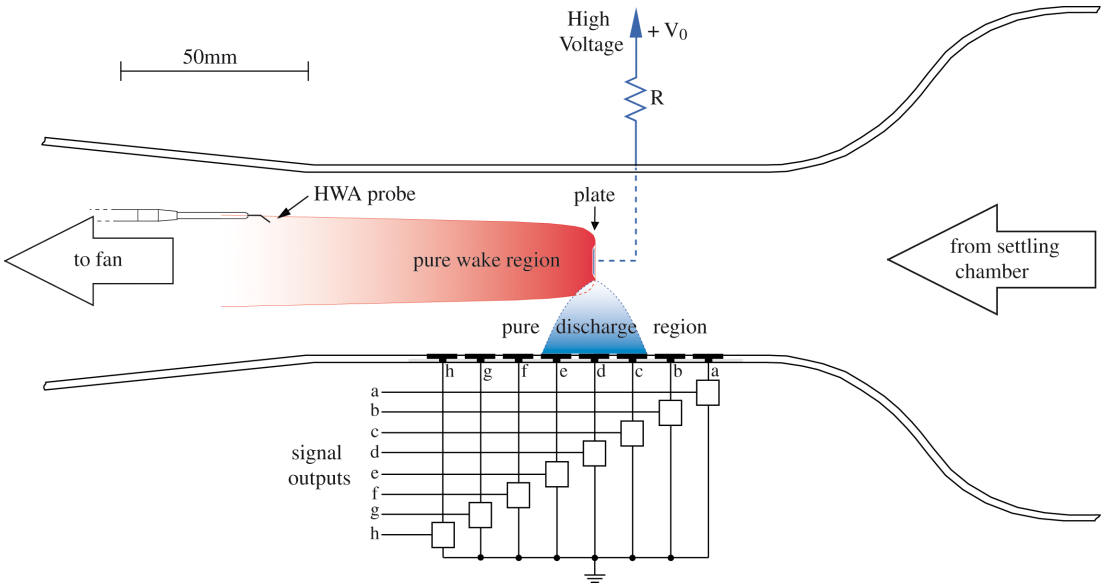


Fig. 2. Experimental setup, scaled coordinates. The flat plate is centered vertically on cathode d). The pure wake zone (without discharge) is sketched by thin lines; the pure discharge zone (without airflow) is sketched by dotted lines. Both regions are described in detail in the body text.

All the tests have been carried out in air at atmospheric pressure, room temperature in the range 293 to 296 K and relative humidity less than 40%. This low humidity range permits a clear identification of the discharge regime, since in general the percentage of water in air is a crucial parameter for the discharges, that may lose stability and reach the spark regime in presence of moisture [26], [27].

A hot wire probe (HW) can be used to measure the velocity power spectrum in the wake. The probe position has been chosen for the best detection of the vortex shedding frequency, minimizing the electromagnetic disturbances originated by the discharge, and is shown in Fig. 2. A probe too close to the anode could also start to act as a cathode and be suddenly destroyed; the discharge–probe distance in the present setup has proven to be safe and is in the order of the distances set by other experimenters [28]. The facilities include also a visualization system, made of a smoke generator working with oil or incense (conductive tracers cannot be used) and two cameras for the visualization of flow and discharge patterns, a CCD color device with VGA resolution and speed of 24 fps and a CMOS B/W device with VGA resolution and speed of 300fps.

## IV. Wake and Discharge Characterization

### A. The pure airstream

The airstream without discharge is a standard case of flow past a bluff body, and in the Reynolds range under consideration it is characterized by a moderate turbulence level. Under these conditions, the velocity fluctuations take place over different time scales, but the main oscillatory behaviour of the wake can be basically characterized by measuring the dominant frequency $f_w$ in the power spectrum of velocities, that is the vortex shedding frequency. The spectrum is obtained from the HW signal acquired at the wake boundary (Fig. 2). The values of this frequency vary approximately from 60 to 130Hz in the considered airspeed range. In dimensionless form, this gives a Strouhal number $St = f_w c/U = 0.168$, that can be compared with the existing literature by accounting for the solid blockage of the plate inserted in the duct. The use of the relevant correction formula [29] leads to a value $St = 0.136$, in very good agreement with the known blockage-free value [30] for the present Reynolds range. Sample measurements are shown in Fig. 3.

### B. The pure discharge

The discharge has a positive polarity and a geometry that can be considered as a 3D generalization of the standard pin-to-plate shape. However, the discharge generated by this geometry exhibits a remarkable difference with respect to the pin-to-plate case. In fact, as electric field and current grow, the pin-to-plate and also other geometries generate at first a proper corona discharge with a current consisting of a DC level plus very high frequency oscillations [5], [7], [9], [10]; then, for higher fields, streamer channels appear, giving rise to strong pulses superimposed to the corona [2], [3]. In the present experiment instead, the discharge arises with the streamer regime, so that the current waveform consists always of strong, separated pulses. This property has been evidenced by suitable visualizations as in Fig. 4, and is coherent with the time histories of the acquired currents; however, it was not clear to the author at the early stage of this investigation, where the standard corona discharge was mentioned as a possible regime in this experiment [25]. The preferential formation of streamer pulses may depend on different causes [1], [6], [31], including the gas composition and the availability of electrons, but in this case the most reasonable cause is the electrodes geometry, and in particular the limited divergence of the electric field at the anodic surface. In general, more than 90% of the streamers hit the cathodes c),d),e) in absence of the airstream, so that the average discharge region can be sketched as in Fig. 2, where

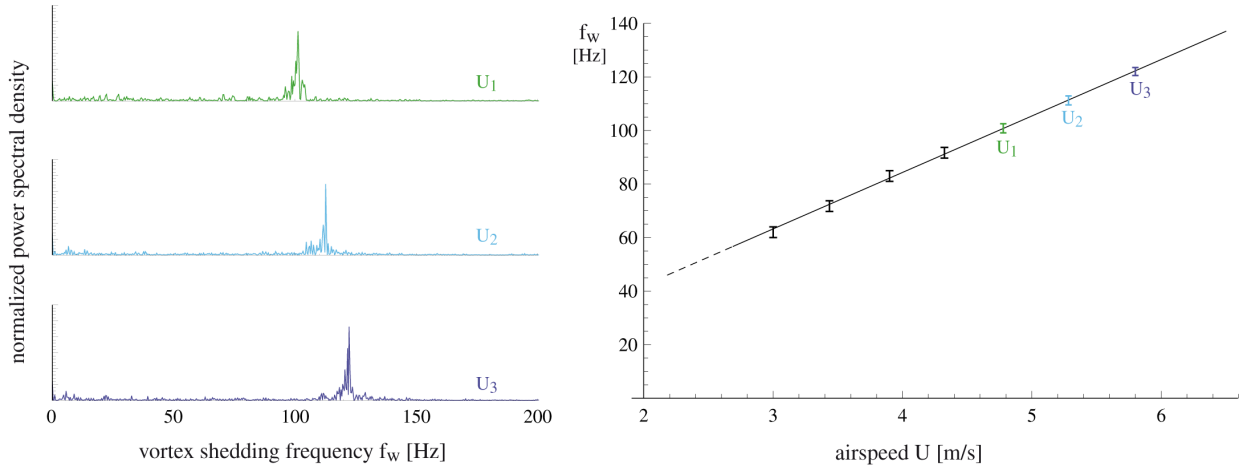


Fig. 3. Measurements of vortex shedding frequencies in the pure flow (without discharge) and relevant interpolation.

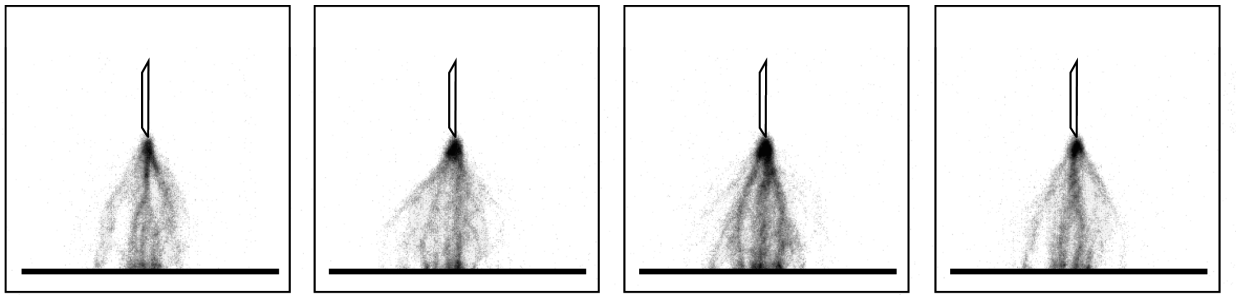

Fig. 4. Pure discharge visualization taken by an intensified camera, B/W inverted images. Selected frames with exposure 3.3ms. The streamer repetition frequency is about 1.5kHz, so that 5 or 6 streamers appear in each frame.

the width of the discharge at the wall is similar to the gap $D$.

Increasing the electric field and consequently the total average current, the number of current pulses per time unit grows, and even the spatial distribution of the pulses changes, as revealed by the multiple cathodes at the test section wall. At low average currents, the bursts arise at first intermittently and only on the cathodes close to the plate (c,d,e). When the total average current overcomes approximately 35 — 40 $\mu$A, the bursts become repetitive, with frequency $f_h$ varying approximately in the range $0.5 < f_h < 5$kHz for currents increasing within the considered range. The frequency $f_h$ is not perfectly stable, but a mean value is measurable by spectral analysis of the cathodic signals, or also by a threshold algorithm performing a direct counting of the bursts, since the current waveforms have in general very high crest factors. At the same time, the spatial distribution of the bursts widens so that for higher currents even the farther cathodes give remarkable signals. In particular, it is interesting to consider the signal on the farther cathodes f),g),h), that play an important role because in the presence of airstream they are located well downstream of the anodic plate. Actually, even in the absence of the airstream, strong repetitive bursts can be observed also on these outputs, but their frequency $f_b$ is remarkably lower than $f_h$, being in general less than 200 Hz.

The phenomena mentioned above are illustrated in Fig. 5, that contains sample time histories for two cathodic currents, $i_c+i_d+i_e$ from the cathodes close to the anode and $i_f+i_g+i_h$ from the farther cathodes. Both currents are shown for the intermittent and the repetitive regimes, corresponding to low and high total average currents. At low total currents, the streamers hit the cathodes c),d),e) creating random positive pulses, whilst the signal from f),g),h) contains very few positive pulses together with weak bipolar pulses due to the capacitive coupling between cathodes (induced peaks are easily identified because of their coherence in phase with the original ones and of their bipolar shape, due to the current–voltage relation across a stray capacitance, $i = C\,dV/dt$). At high total currents, the streamers hit repetitively the cathodes c),d),e) giving positive pulses with frequency $f_h$ and the cathode f) giving positive pulses with the lower frequency $f_b$. Again, there are induced peaks, visible as strong negative pulses on the upper curve, and small bipolar pulses in the lower curve.

## V. Results

The interaction of airstream and discharge in the present setup gives rise to several phenomena. As a first step, a smoke wire visualization can give useful information: it reveals that the wake patterns are deflected toward the cathodic wall, this phenomenon is particularly evident on the vortex shed periodically on the discharge side. The reason for this deflection is the electric wind, directed from the anode to the cathodic wall, created by the repetitive streamers. The air motion originated in this way is similar to the one created by a stable corona

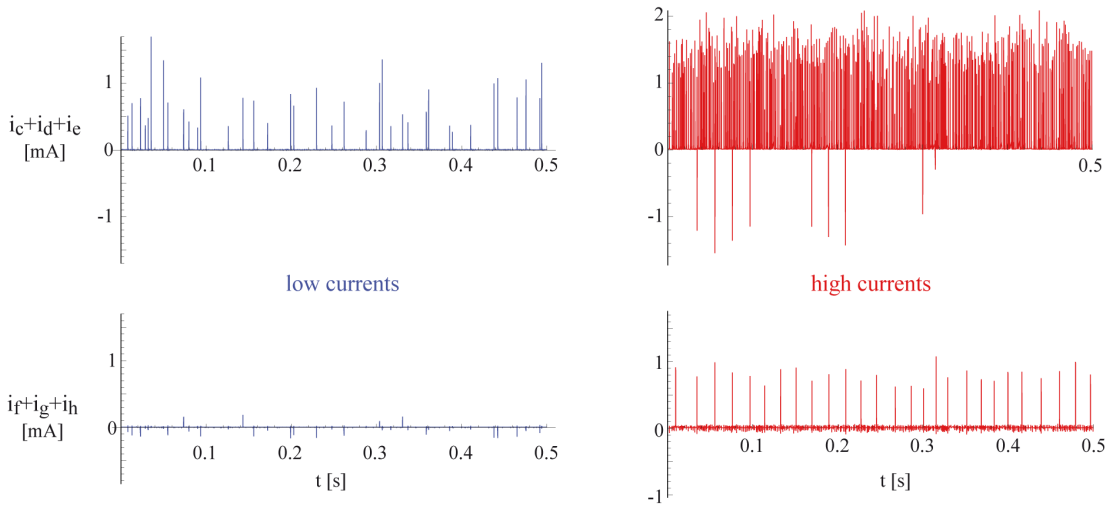


Fig. 5. Current waveforms for different discharge currents, cumulative outputs from cathodes c),d),e) and f),g),h), no airstream. Left panels: low current regime, average total current $= 20\mu$A; right panels: high current regime, average total current $= 55\mu$A, repetition frequencies $f_h$=720Hz (upper panel) and $f_b$=54Hz (lower panel). The frequency fluctuations are in the order of $0.1\,f_h$ and $0.3\,f_b$.

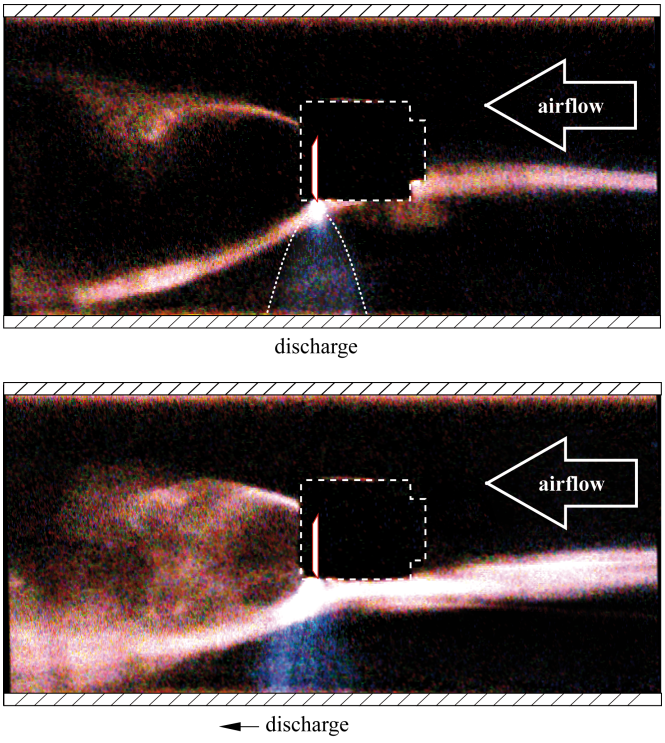


Fig. 6. Visualization of flow and discharge deflections. Airflow shown by smoke wire technique. The dashed line is the contour of an insulator. The first image evidences the flow deflection (the contour of the discharge is approximately sketched by dotted lines), whereas the second image evidences the discharge deflection. The exposure is 10ms and $f_h \simeq 2.1$kHz, thus a mean number of 21 streamers appears in each frame.

discharge [11], [32], and in the absence of the axial airstream it should give rise to a large region of recirculating flow.

Even the discharge is deflected by the axial airflow, toward the downstream direction. The morphological changes of discharge and airstream can be considered over different time scales: over times much longer than the largest scale ($\gg 1/f_w$, in the order of 1s), only the deflected average contours of the wake and the discharge can be seen. On the other hand, over short times ($\sim 1/f_h$, or less than 1ms), the structures of streamers and vortices can be identified, but they change continuously. As a further choice, the Fig. 6 presents a visualization based on intermediate time scales (exposure=10ms). In this way, the single streamers are not resolved and only the envelope of the discharge is shown, whereas the wake structure is roughly visible. Two frames selected from the same movie are shown, the first one highlights the flow deflection and the second one, including at least one streamer directed to a downstream cathode, highlights the discharge deflection. This visualization has been obtained with $U$=3.2m/s and a current discharge of 100$\mu$A, giving $N_{\mathrm{EHD}} \sim$0.5, so that the effects of airflow and discharge are somewhat balanced. The vortex shedding is visualized by incense smoke, whereas the discharge is automatically visible thanks to its light emission.

An examination of different visualizations over long time scales shows that these deflections are related to the values of discharge current and flow velocity as expressed by the $N_{\mathrm{EHD}}$ number: the discharge deflection increases for lower $N_{\mathrm{EHD}}$, whereas the wake deflection increases for higher $N_{\mathrm{EHD}}$. In the present range of $N_{\mathrm{EHD}}$ a complete vortex shedding suppression has not been observed.

Quantitative information about the airflow–discharge interaction can be obtained by analyzing the signals of the HW and of the current outputs. A first examination of the HW spectra under the effect of the gas discharge does not reveal major changes, only the amplitude of the main peak may vary in some cases. This effect will be discussed later.

A more complicated change can be detected by analyzing the time histories of the cathodic currents under the effect of the airstream. The total current, above the cited threshold of about 40$\mu$A, has in general a waveform made of fast pulses at frequency $f_h$. As $U$ increases, the amplitudes of the outputs a),b),c) decrease rapidly whilst the outputs d)... f) maintain a good level. Even under the influence of the airstream, the

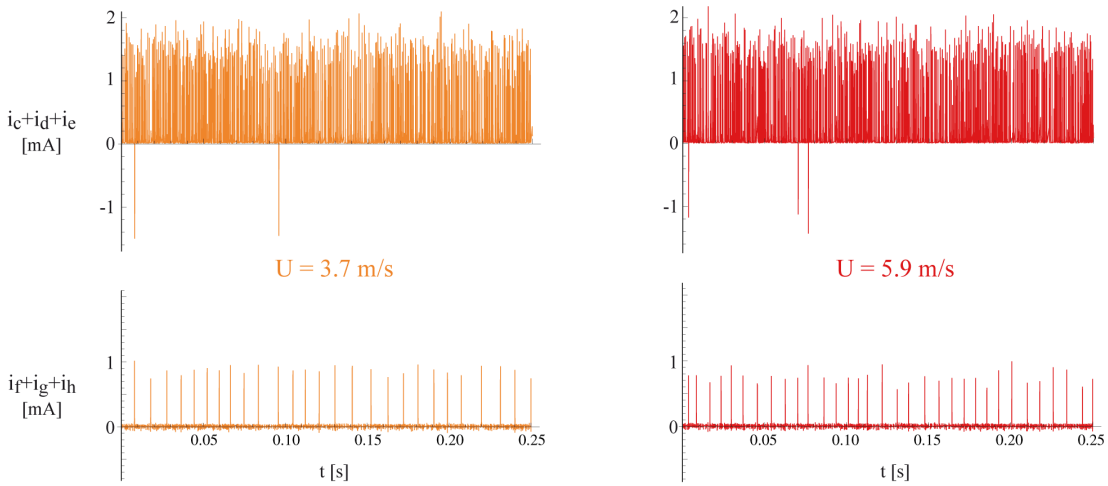


Fig. 7. Current waveforms for different airstream velocities at the same average total current = 100 $\mu$A. Cumulative outputs from cathodes c),d),e) and f),g),h). Left panels: lower velocity, frequencies $f_h$=2.1kHz (upper panel) and $f_b$=104Hz (lower panel); right panels: higher velocity, frequencies $f_h$=2.1kHz (upper panel) and $f_b$=131Hz (lower panel). Fluctuations are in the order of $0.05\,f_h$ and $0.1\,f_b$.

waveforms of cathodes d) and e) remain characterized by pulses at frequency $f_h$ typically in the kHz range, whereas the outputs f),g),h) contain sharp peaks at frequency $f_b$, always below 200Hz. The waveforms of the cathodes g),h) are similar to the one of f) but with smaller amplitudes. As explained in §IV-B, each waveform contains also peaks due to capacitive couplings, but they are easily identifiable so that do not prevent the correct interpretation of the results. As for the pure discharge, the signal sums $i_c + i_d + i_e$ and $i_f + i_g + i_h$ are a good source of information, and permit easy measurements of the high and low frequencies $f_h$ and $f_b$. As observed in the absence of the airstream, both frequencies depend on the discharge regime, i.e. on the total average current, increasing for higher currents. However, for $U \neq 0$, the high frequency $f_h$ appears nearly airspeed–independent (only a very weak decrease of $f_h$ can be observed for increasing $U$) whilst the low frequency $f_b$ turns out to increase with the flow velocity $U$. An example is reported in Fig. 7.

The dependency of the low frequency $f_b$ on current and airspeed suggests to compare these measurements under different flow and discharge conditions: this can be done as in Fig. 8, where the $f_b$ curves are recorded as functions of the total time-averaged discharge current and of the airspeed. This figure contains 5 curves of this kind, identified by the total currents $i_n$ measured at $U = 0$ m/s. The vortex shedding frequency of the wake is also plotted in the same figure. The lowest curve 1) is acquired for low currents, in the upper range of intermittence, so that the values of $f_b$ are affected by large fluctuations and below this level they cease to be measurable. Along this curve only a slight increase of $f_b$ can be observed at high airspeeds. The curve 2) starts at a frequency slightly higher than curve 1), but the trend is very different: here the frequency gets close to the wake frequency along a visible range of flow velocities, this phenomenon stops at the highest values of $U$. The curve 3) is similar, and in this case $f_b$ seems to be strongly attracted by the wake frequency $f_w$. A similar behaviour, shifted to higher values of $U$, can be observed in curve 4). The curve 5) returns to be only slightly modified by the airspeed, and for

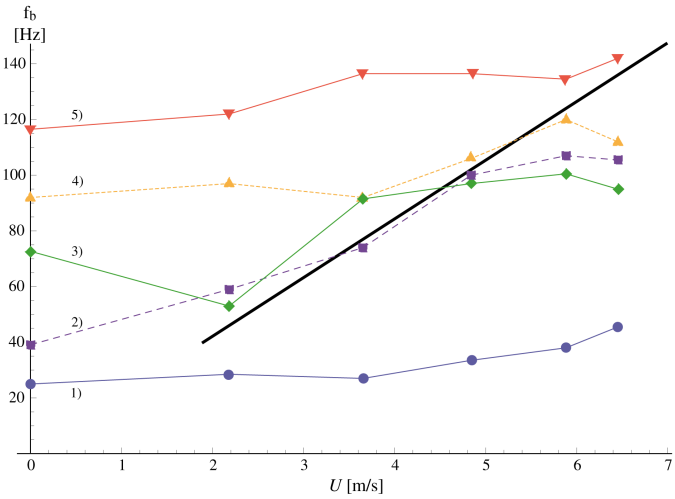


Fig. 8. Vortex shedding frequency $f_w$ (thick line) and discharge burst frequencies $f_b$ for 5 current levels, identified by the total time-averaged discharge currents $i_n = 29, 40, 68, 87, 106\mu$A measured at $U = 0$ m/s. The fluctuations of the measured $f_b$ values are reported in the body text. The wake frequency is measured with accuracy $\pm 1.5$ Hz, and represents the wake with and without discharge.

higher currents the appearance of transient sparks becomes increasingly probable. The intermediate curves 2), 3), 4) have parts close to the wake frequency, this fact could be considered as a strong interaction, probably a coupling phenomenon.

The data set used for Fig. 8 has been obtained by repeating a defined procedure: at first the airspeed is set to a stable value, then the discharge current is varied by adjusting the power supply in stepwise mode. Each point is a mean value calculated on repeated tests, the relevant variation interval ranges from $\pm$7Hz to $\pm$16Hz, with the lowest variations occurring for $f_b$ close to the wake frequency $f_w$ and for the highest values of $U$ and $f_b$. Technically, these values are not just measurement accuracies, since they are influenced, besides the measurements technique, by the inherently low stability of the frequency $f_b$, that worsens at the lower frequencies and at

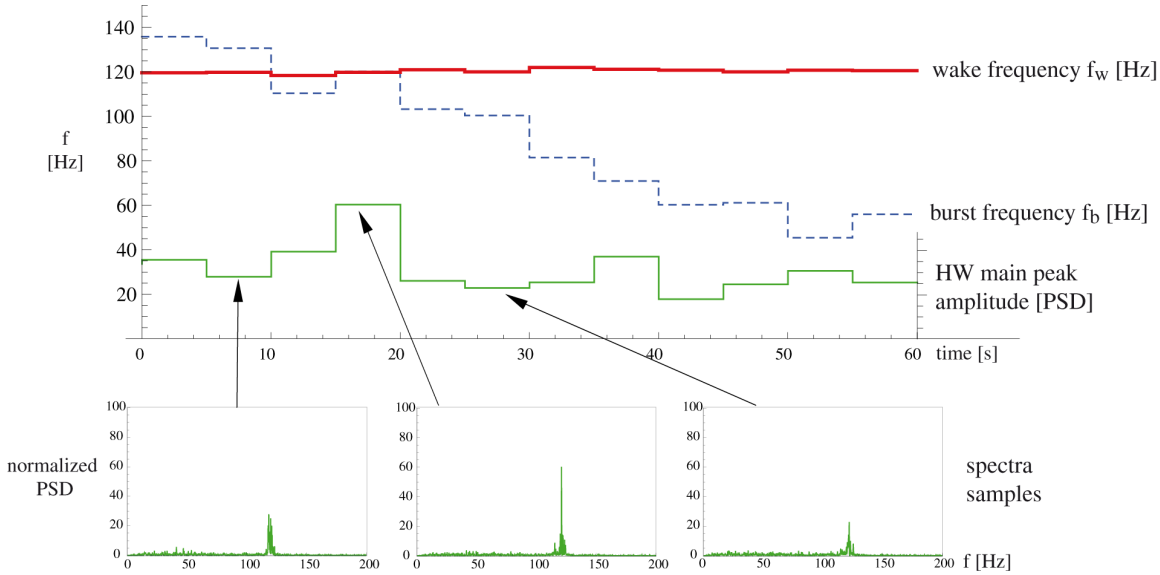


Fig. 9. Coupling identification by analysis of the peak height in the HW spectrum, for constant $U$ and total current lowered in stepwise mode.

the lower velocities.

A further investigation on this phenomenon can be carried out examining the properties of the waveforms of velocity and currents both in the coupled and the uncoupled ranges. Actually, the coupled range can be detected on the current signals by looking at the frequency $f_b$, which is clearly modified by the interaction with the wake as in Fig. 8. However, the effects of the coupling are not so evident on the wake frequency, that seems to remain unchanged in presence and absence of the discharge, within the measurement accuracy. In fact, it has been verified that the vortex shedding frequency plotted in Fig. 8 may represent both the cases. A check of the phase relation between velocity and current signals could be theoretically done, but is quite difficult, because of the very different waveforms of the two time series; in particular, even if the high crest factor of the current signals permits an identification of each burst, the velocity signal is quite smooth and different methods of phase analysis may lead to conflicting results.

A different approach to the problem may be tried as follows. Simultaneous time series of HW velocity and currents can be acquired by varying a control parameter (airstream velocity or total discharge current), in such a way as to record subsequent parts with coupled and uncoupled signals. The appearance of the velocity waveforms does not exhibit any particularity during the supposed coupling time window, except an amplitude variation, not easy to observe directly, but easy to check in the frequency domain. In fact, a comparison of the spectra extracted from time windows with and without coupling reveals a reinforcement of the main peak at frequency $f_w$ during the coupling time. A spectral criterion for the velocity can then be introduced by checking the height of the spectral peak in the HW signal. Actually, the time history of the main peak height obtained from subsequent signal spectra (here taken over 5 s and shifting the starting time of a rectangular window by increments of 5 s), confirms that the peak reaches a maximum value under coupling conditions. An example is shown in Fig. 9, where the airspeed is kept constant at $U = 5.9$m/s and the total discharge current is progressively lowered in stepwise mode from $110\mu A$ to $50\mu$A. It is easy to prove that the increase of the main peak is not due to an EM disturbance induced by the discharge, since this one should be always visible even outside coupling. Furthermore, the resulting spectrum in that case would be definitely different, owing to the presence of many harmonics of the frequency $f_b$.

## VI. Discussion and Conclusions

### A. The frequency $f_h$ for $U = 0$

The bursts are characterized by high current values, appearing as peaks of very short duration. Short exposure visualizations as in Fig. 4 reveal that the bursts are essentially streamers. Each streamer connects a point along the anode tip to a point on the cathodic wall. Their waveform, as reported in other works, is characterized here by a fast rise time followed by a relaxation phase; the rise time, typically less than 100ns, cannot be resolved safely by the present setup, so that the pulses are essentially revealed by reading their decaying phase. As a consequence, the peak values of the recorded currents may have a low accuracy, whereas the measured frequencies have reliable values. The repetition of DC driven streamers is reported in many works, and is generally believed to depend on the gas and on the electric circuit properties: after the passage of a streamer through the gap, the gas returns to its initial properties and a new streamer can start as soon as the circuit has enough energy to generate it.

In the simplest model, the circuit parameters involved are expressed by the ballast resistance $R$ and the total capacitance $C$ of electrodes and cables. Obviously, the characteristic time of this circuit is $RC$, that gives in this setup a scale frequency $1/RC \sim 1.5$kHz, within the observed range of $f_h$. This model can be refined as follows: the capacitance $C$ is charged through $R$ and as the voltage increases, when a given threshold

voltage $V_t$ is reached, a burst is generated by discharging the capacitance abruptly. The charging voltage can be expressed by the simple law

$$V(t) = V_0[1 - \mathrm{e}^{-\frac{t}{RC}}] \tag{6}$$

and the burst appears when $V(t) = V_t$, i.e. at time

$$\tau = R\,C \ln \frac{V_0}{V_0 - V_t}. \tag{7}$$

This is a time scale whose inverse $1/\tau$ should give a more accurate frequency scale for the bursts, as function of $V_t$. Actually, the value of the threshold $V_t$ is not easy to calculate or measure, since it depends on the gas properties like temperature and residual ionization (similar problems are treated by Janda et al. [33] and Korolev et al. [18] for different geometries and current ranges), but supposing a reasonable range for $V_t$, eq. (7) may account for the variations of $\tau$ and of the relevant frequency. For example, assuming $0.5 < V_t < 0.95V_0$, with the values of $R, C$ and $V_0$ of the present setup, the frequency scale turns out to be between 0.5 and 2.5kHz, in good agreement with the observed $f_h$ range. The higher frequencies can be reached when the anode-cathode gap does not completely recover its dielectric strength after a burst, so that the value of $V_t$ remains low and the next burst can start after a shorter time. This effect could be related to the local increase of gas temperature and decrease of gas density caused by the streamers, originating small regions of lower dielectric strength (see [32] for streamers, [33] for higher currents). However, as described and explained below (§VI-C), the frequency $f_h$ is only slightly modified by the passage of new gas through the gap when the airflow is on.

### B. The frequency $f_b$ for $U = 0$

About the lower frequency $f_b$ observed in this experiment, another mechanism is involved, related to the spatial distribution of the discharge current. This distribution is well known for the famous case of the pin-to-plate corona discharge, where the current density behaves as $\cos^m \theta$ with $m \simeq 5$ and $\theta$ is the angle between the pin tip and any point on the plane (Warburg law). In the present case the geometry is different and the discharge is made of streamers, however it is known that in similar cases the distribution becomes more peaked [34]. Furthermore, a rough discretization of the distribution is obtained here thanks to the multiple cathodes: the mean currents recorded on outputs d),e),f),g),h) normalized on the highest value of cathode d) are proportional to (1, 0.18, 0.06, 0.03, 0.01) with 10% accuracy within a large range of total currents, and this may give a criterion about the occurrence of a streamer on each cathode (the values of a),b),c) are symmetric for $U = 0$). Assuming on a statistical basis that the streamer frequency on each cathode is directly proportional to the value reported above, the expected scale for the bursts frequency on cathode f) should be $f_b \simeq 0.06 f_h$, i.e. very close to the observed range.

The random appearance of bursts on the farther cathodes may also explain the relatively high fluctuations of $f_b$, particularly without airstream; another phenomenon that affects the stability of $f_b$ (and also of $f_h$) is the fact that each streamer is originated by a different point along the anode edge, as may happen in other 3D geometries like the wire-to-plane and wire-to-cylinder.

### C. Interactions for $U \neq 0$

Obviously, the presence of a transverse airflow causes a modification of the scenario depicted above. The electric wind interacts with the imposed airstream to generate a new unsteady flow configuration, as sketched in Fig. 6 and described in the relevant body text. The results of §V can be outlined by reporting that the velocity fluctuations are influenced in amplitude but not in frequency, whereas the discharge frequencies measured over different spatial locations are modified. Under the influence of the airstream the time-averaged current profile along the wall, as expected, is shifted downstream, so that the outputs a),b),c) decrease remarkably, and the outputs e),f),g),h) increase progressively.

In particular, the two discharge frequencies under study are influenced to different extents. The burst repetition frequency $f_h$, related to the electric field, to the circuit parameters, and to the gas properties, is nearly airspeed-independent and only weakly lowered by the imposed airflow in some tests. More specifically, the electric parameters remain the same, but the input of new air in the gap could restore the electric rigidity faster and bring to longer times between bursts: however, this phenomenon is not observed. It is likely that the zones of higher temperature at the anode and at the wall are only slightly affected by the airflow, because of the boundary layer and, for the anode, because of the locally high electric field.

The effect on the lower frequency $f_b$ is definitely different, since under these conditions a larger number of streamers is distorted and shifted toward the peripheral cathodes. This gives rise, besides the mentioned increase in the local average current, to an increase of $f_b$ related to the increase of $U$. In general, the dependence of $f_b$ on $U$ is not strong, unless $f_b$ and $U$ are in the coupling range, as exposed in §V. In this range, the data show that the time-dependent behaviour is mainly driven by the fluid dynamics, since the wake frequency $f_w$ is not influenced by the discharge, whilst the burst frequency $f_b$ undergoes a large change. Furthermore, under these conditions, not just the time scale $\tau \sim 1/f_b$ becomes similar to the vortex shedding period $1/f_w$: even the time scale $\Delta x/U$ for the transport of a fluid particle or ion over the space $\Delta x$ between cathodes d) and h) approaches $\tau$ and $1/f_w$. A mechanism compatible with the data and the scales exposed above can be described by assuming that the streamers reaching the farther cathodes are emitted during the roll-up time of each new vortex on the cathodic side, because this phenomenon favors the transport of ionized gas along the cathodic wall direction. This description may also include a sort of feedback mechanism, since the electric wind due to the longer streamers emitted at $f_b \sim f_w$ can reinforce the velocity fluctuations of the vortex shedding by acting in phase with them, and giving rise to the observed higher peak in the velocity spectrum. Even the smaller deviations from the mean value of $f_b$ in the coupling range are consistent with the present description.

Finally, these considerations should be also regarded from the point of view of dimensional analysis, as outlined in §II: it turns out that for $N_{\mathrm{EHD}}$ numbers in the order of the unity, both the morphologies of the wake and the discharge are modified as a consequence of the reciprocal influence. In the time domain instead, each actor maintains its own characteristic main frequency ($f_w$ and $f_h$) and when a coupling is detected, the second discharge frequency $f_b$ approaches the dominant frequency given by the wake.

## REFERENCES


[1] L.B. Loeb, *Electrical Coronas, Their Basic Physical Mechanisms*. University of California Press, Berkeley, CA, 1965.

[2] C.F. Gallo, "Corona – A Brief Status Report", *IEEE Trans. Ind. Appl.* IA-13 no. 6: 550–557, 1977.

[3] M. Goldman, A. Goldman and R.S. Sigmond, "The corona discharge, its properties and specific uses", *Pure & Appl. Chem.* vol. 57 no. 9, 1353–1362, 1985.

[4] J.S. Chang, A. Watson, "Electromagnetic hydrodynamics", *IEEE Trans. Dielectr. Electr. Insul.* vol. 1 no. 5, 871-895, 1994.

[5] A. Fridman, A. Chirokov and A. Gutsol, "Non-thermal atmospheric pressure discharges", *J. Phys. D: Appl. Phys.* vol. 38, R1-R24, 2005.

[6] R.T. Waters and W.B. Stark, "Characteristics of the stabilized glow discharge in air", *J. Phys. D: Appl. Phys.*, vol. 8, 416–427, 1975.

[7] J.E. Jones, A. Boulloud and R.T. Waters, "Dimensional analysis of corona discharges: the small current regime for rod-plane geometry in air", *J. Phys. D: Appl. Phys.* vol. 23, 1652–1662, 1990.

[8] M. Cernak, T. Hosokawa and M. Inoshima, "Positive–streamer–like phenomena in point–plane corona gaps: Trichel pulses and high pressure cathode sheath instabilities", *Appl. Phys. Lett.* vol. 57 no.4, 339–340, 1990.

[9] R. Morrow, "The theory of positive glow corona", *J. Phys. D: Appl. Phys.* vol.30, 3099-3114 , 1997.

[10] R.S. Sigmond, "The Oscillations of the Positive Glow Corona", *J. Phys. IV France* vol.7, Colloque C4, Supplement au Journal de Physique III d'octobre 1997, C4–383–395, 1997.

[11] J.F. Loiseau, J. Batina, F. Noël and R. Peyrous, "Hydrodynamical simulation of the electric wind generated by successive streamers in a point-to-plane reactor", *J. Phys. D: Appl. Phys.* vol.35, 1020-1031, 2002.

[12] Y.D. Korolev, O.B. Frants, V.G. Geyman, V.S. Kasyanov and N.V. Landl, "Transient Processes During Formation of a Steady-State Glow Discharge in Air", *IEEE Trans. Plasma. Sci.* vol.40, no. 11, 2951-2960, 2012.

[13] S.R. Li, I.V. Timoshkin, M. Maclean, S.J. MacGregor, M.P. Wilson, M.J. Given, J.G. Anderson, T. Wang, "Steady-State Corona Discharges in Atmospheric Air for Cleaning and Decontamination" *IEEE Trans. Plasma. Sci.* vol.41, no. 10, 2871-2878, 2013.

[14] E. Moreau, "Airflow control by non–thermal plasma actuators", *J. Phys. D: Appl. Phys.* vol.40, 605–636, 2007.

[15] Yu Akishev, O. Goossens, T. Callebaut, C. Leys, A. Napartovich and N. Trushkin, "The influence of electrode geometry and gas flow on corona-to-glow and glow-to-spark threshold currents in air", *J. Phys. D: Appl. Phys.* vol.34, 2875-2882, 2001.

[16] Yu Akishev, M. Grushin, V. Karalnik, A. Petryakov and N. Trushkin, "Non-equilibrium constricted dc glow discharge in $N_2$ flow at atmospheric pressure: stable and unstable regimes", *J. Phys. D: Appl. Phys.* vol.43, 075202, 11pp, 2010.

[17] J. Podlinski, A. Niewulis and J. Mizeraczyk, "Electrohydrodynamic flow in a wire-plate non-thermal plasma reactor measured by 3D PIV method", *Eur. Phys. J. D* vol.54, 153–158, 2009.

[18] Y.D. Korolev, O.B. Frants, N.V. Landl, V.G. Geyman and I.B. Matveev, "Glow-to-Spark Transitions in a Plasma System for Ignition and Combustion Control", *IEEE Trans. Plasma. Sci.* vol.35, no. 6, 1651-1657, 2007.

[19] Y. Xian, X. Lu, S. Wu, P.K. Chu and Y. Pan, "Are all atmospheric pressure cold plasma jets electrically driven?", *Appl. Phys. Letters* vol.100, 123702, 2012.

[20] Y.D. Korolev, O.B. Frants, N.V. Landl, A.I. Suslov, "Low-Current Plasmatron as a Source of Nitrogen Oxide Molecules", *IEEE Trans. Plasma. Sci.* vol.40, no. 11, 2837-2842, 2012.

[21] X.J. Shao, Z.S. Chang, H.B. Mu, W.L. Liao, G.J. Zhang, "Experimental and Numerical Investigation on the Interaction Between Ar Flow Channel and Ar Plasma Jet at Atmospheric Pressure", *IEEE Trans. Plasma. Sci.* vol.41, no. 4, 899-906, 2013.

[22] IEEE-DEIS-EHD Technical Committee, "Dimensionless parameters for EHD flow", *IEEE Trans. DEI* vol.10, 3-6, 2003.

[23] S. Soldati and S. Banerjee, "Turbulence modification by large scale organized electrohydrodynamic flows", *Phys. Fluids* vol.10 no.7, 1742–1756, 1998.

[24] P. Magnier, D. Hong, A. Leroy-Chesneau, J. Bauchire and J. Hureau, "Control of separated flows with the ionic wind generated by a DC corona discharge", *Exp. in Fluids* vol.42, 815–825, 2007.

[25] M. Belan, "A gas discharge normal to a wake: experimental investigation of the plasma-flow interaction", in *Progress in Turbulence V*, A. Talamelli et al. (eds), Springer Proc. in Phys. 149, 153–157, 2013.

[26] C. Louste, E. Moreau and G. Touchard, "Influence of an insulating flat plate on a DC surface corona discharge at various air relative humidity", in *Electrostatics, Inst. of Phys. Conf. Series* vol.178, 273-278. Bristol: Inst. of Phys. Publishing, 2004.

[27] M. Rickard, D. Dunn-Rankin, F. Weinberg and F. Carleton, "Maximizing ion-driven gas flows", *J. Electrostatics* vol.64, 368-376, 2006.

[28] J.S. Chang, J. Ueno, H. Tsubone, G.D. Harvel, S. Minami and K. Urashima, "Electrohydrodynamically induced flow direction in a wire-non-parallel plate electrode corona discharge", *J. Phys. D: Appl. Phys.* vol.40, 5109-5111, 2007.

[29] T. Ota, Y. Okamoto and H. Yoshikawa, "A correction formula for wall effects on unsteady forces of two-dimensional bluff bodies", *J. Fluids Eng.* vol.116: 414–418 , 1994.

[30] J.M. Chen and Y.C. Fang, "Strouhal numbers of inclined flat plates", *J. Wind Eng. Ind. Aerodyn.* vol.61: 99-112, 1996.

[31] D.Z. Pai, D.A. Lacoste and C.O. Laux, "Transitions between corona, glow, and spark regimes of nanosecond repetitively pulsed discharges in air at atmospheric pressure", *J. Appl. Phys.* vol.107, 093303, 2010.

[32] H. Tajalli, D.W. Lamb and G.A. Woolsey, "Energy transfer in positive streamers", *J. Phys. D: Appl. Phys.* vol.22 1497–1503, 1989.

[33] M. Janda, V. Martišovitš and Z. Machala, "Transient spark: a dc-driven repetitively pulsed discharge and its control by electric circuit parameters", *Plasma Sources Sci. Technol.* vol.20, 035015, 2011.

[34] M. Boutlendj and N.L. Allen, "Current-density Distribution on a Plane Cathode in DC Glow and Streamer Corona Regimes in Air", *IEEE Trans. Electr. Insul.*, vol. 28 no. 1, 86–92, 1993.


**Marco Belan** He received his MSc. in Physics in 1991 from Universitá di Torino and his Ph.D. in Aerospace Engineering in 1995 from Politecnico di Torino. He has been working in the Aerodynamics Laboratory of the Aerospace Engineering Department, Politecnico di Milano, since 1999. He is now faculty researcher, appointed for the MSc course of experimental fluid dynamics. His research topics include experiments on turbulent drag reduction, bluff body wakes, hypersonic jets and works in the field of applied mathematics.